AISI-304 STAINLESS STEEL THIN-WALLED TUBE HOLLOW SINKING PROCESS PARAMETERS ORTHOGONAL OPTIMIZATION STUDY

Jinfeng ZHANG[1], Chunjiang ZHAO[1*], Bijuan YAN[1], Yiwei XU[1], Qiang BIAN[1]

To address a series of problems caused by improper drawing parameters of small-diameter stainless steel thin-walled tubes, this paper selects AISI-304 stainless steel tubes of φ2mm×0.1mm×140mm as the research object. The finite element model is established, and the forming process is simulated using the DEFORMÂ® Software. The effects of different process parameters, such as drawing speed, friction coefficient, and outer die angle on the damage, maximum effective stress, and pulling force were analyzed. Finally, the process was optimized using orthogonal experiments. The results show that the optimized parameters combination is the drawing speed of 30 mm/s, the friction coefficient of 0.05, and the outer die angle of 12°. With this combination of parameters, the maximum effective stress, damage and pulling force were reduced by 3.8%, 21.82% and 12.52% respectively, which improved the surface quality of the tubes and provided a theoretical basis for the optimization of hollow sinking.

Keywords: stainless steel tubes; hollow sinking; process parameters; drawing force; orthogonal optimization

1. Introduction

Stainless steel thin-walled tubes have a wide range of applications in nuclear power, medical, heat exchangers, and other fields. According to the production method, it can be divided into seamless tubes and welded tubes [1-2]. Among them, the seamless tube can withstand high pressure, while the welded tube can not withstand too much pressure due to the poor pressure-bearing capacity at the weld seam. And 304 stainless steel thin-walled tube in the aerospace industry is mainly used as a fluid container liquid tube line [3]. Therefore, the study of the 304 stainless steel seamless thin-walled tube production process has been an important direction to explore and improve the stainless steel tube as well as the subject to be solved.

The methods of processing seamless tubes are rolling, extruding, and drawing. Of these, drawing is the most widely used method. Drawing methods are

[1] Mr., School of Mechanical Engineering College, Taiyuan University of Science and Technology, China, e-mail: zjf15735044589@126.com.
[*] E-mail: zhaochj75@163.com.

usually divided into hollow sinking, drawing with a core, fixed core head drawing, and traveling core head drawing [4-5]. As the stainless steel tubes under study are characterized by small outer diameter and thin wall thickness, the hollow sinking method is used. The biggest problem with hollow sinking is that the tube is internally free deforming, with no support on the inside wall, and prone to surface defects and other problems [6]. In recent years, researchers at home and abroad have conducted a lot of research on the hollow sinking process. For example, Wang et al [7] studied the effect of air-drawing speed on the surface quality, mechanical properties, and dimensional accuracy of zinc alloy micro-tubes. Xie et al [8] studied the characteristics of the medium effect force-strain, and velocity distribution in the air-drawing process of seamless steel tubes, which provided a basis for conducting the design of the air-drawing steel tube process. Jin, Xia, and Faeahani et al [9-11] investigated hollow sinking dies, providing a theoretical basis for predicting and optimizing die life. Gattmah, Boutenel, et al [12-13] investigated the effect of die half-angle on drawing forces and tube geometry. As residual stresses have a significant influence on the quality of the tube product, other scholars have investigated the effect of residual stresses on the tube drawing process [14-16]. However, the mechanism of the effect of different process parameters and combinations on the hollow sinking of small-diameter stainless steel thin-walled tubes is not clear.

Therefore, this paper firstly establishes the kinetic equations of the empty drawn tube. Using the DEFORMÂ® Software, a finite element model of hollow sinking was established to investigate the influence of different drawing speeds, friction coefficients, and outer die angles on the maximum Effective stress, damage factor, and drawing force. Finally, the influence of the process parameters was ranked by the orthogonal optimization method. The best ratio of the process parameters was obtained. The research results of this paper can provide some reference for the application and parameter selection of the hollow sinking process in various tube billets.

2. Kinetic equations for air-drawn tubes

When the tube is pulled empty, the outer forces are shown in Fig. 1(a). The tube is moved forward by the pulling force P. As the outer die compresses the tube, the tube is subjected to the pressure N of the outer die and the frictional force T generated by it. At this point, a tiny unit body is taken in the plastic deformation zone and its state of stress is shown in Fig. 1(b). The following assumptions are made: the wall thickness of the drawn tube is constant and the stress distribution is uniform within a certain range; the normal compressive stress σ_n on the inner and outer surfaces of the embryo is equal in the reduced wall

section of the tube when it is pulled empty, and the coefficient of friction f is the same.

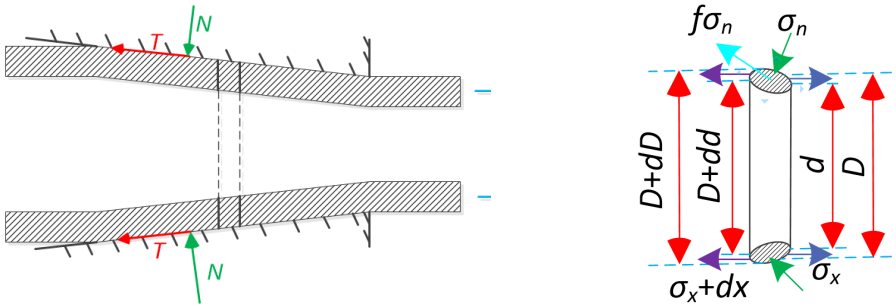

(a) (b)

Fig.1 The force of the tube when it is pulled empty

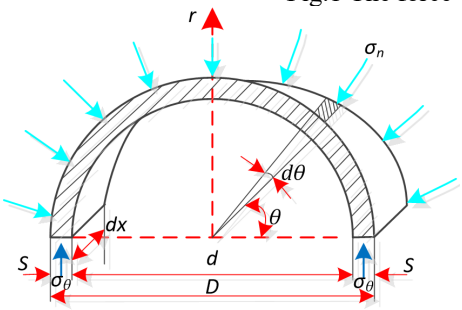

Fig.2 The relationship between σ_θ and σ_n

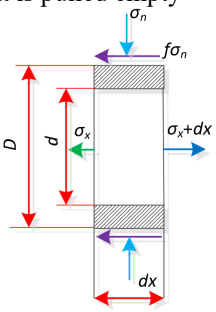

Fig.3 Stress state of the tiny unit body in the sizing area

As shown in Fig. 1(b), micro-units of thickness dx is taken in the deformation zone.

The differential equilibrium equation established in the axial direction can be written as:

$$(\sigma_x + d\sigma_x)\frac{\pi}{4}\left[(D+dD)^2-(d+dD)^2\right]-\sigma_x\frac{\pi}{4}(D^2-d^2)+\frac{1}{2}\sigma_n\pi DdD+\frac{f\sigma_n\pi D}{2\tan\alpha}dD=0 \quad (1)$$

where σ_x is the axial tensile stress; σ_n is the radial compressive stress; D is the outer diameter of the tube; d is the inner diameter of the tube; α is the mold angle of the outer mold, and f is the coefficient of friction.

Expanding and simplifying Eq. (1) and ignoring the higher order differentials, which can be expressed as:

$$(D^2-d^2)d\sigma_x+2(D-d)\sigma_x dD+2\sigma_n DdD+2\sigma_n D\frac{f}{\tan\alpha}dD=0 \quad (2)$$

The introduction of the plasticity condition is given as follows:

$$\sigma_x + \sigma_\theta = \sigma_s \tag{3}$$

where σ_θ is the circumferential compressive stress; σ_s is the deformation resistance of the tube.

From Fig. 2, the equilibrium equation established in the r direction can be obtained:

$$2\sigma_\theta S dx = \int_0^x \sigma_n \frac{D}{2} d\theta dx \sin\theta \tag{4}$$

where S is the wall thickness of the tube.

Eq. (4) can be simplified as:

$$\sigma_\theta = \frac{D}{D-d}\sigma_n \tag{5}$$

Eq. (3) and Eq. (5) are substituted into Eq. (2), and according to the boundary conditions, which can be expressed as:

$$\frac{\sigma_{x1}}{\sigma_s} = \frac{1+B}{B}\left(1-\frac{1}{\lambda^B}\right) \tag{6}$$

where λ is the elongation factor of the tube; $B = f/\tan\alpha$.

Fig. 3 shows a unit removed from the calibrating straight, the differential equilibrium equation established along the axial direction can be described as:

$$\left(\sigma_x + d\sigma_x\right)\frac{\pi}{4}(D_1^2 - d_1^2) - \sigma_x \frac{\pi}{4}(D_1^2 - d_1^2) - f\sigma_n \pi D_1 dx = 0 \tag{7}$$

where D_1 is the outer diameter of the tube in the calibrating straight; d_1 is the inner diameter of the tube in the calibrating straight.

Eq. (7) can be simplified as:

$$\frac{1}{4}\left(D_1^2 - \mathrm{d}_1^2\right) d\sigma_x = f\sigma_n D_1 dx \tag{8}$$

The introduction of the plasticity condition is given as follows:

$$\sigma_x + \sigma_n = \sigma_s \tag{9}$$

Substituting Eq. (9) into Eq. (8), the following relationships could be gotten as:

$$\frac{d\sigma_x}{\sigma_s - \sigma_x} = \frac{4fD_1}{\left(D_1^2 - d_1^2\right)} dx \tag{10}$$

Integrating Eq. (10) over the long range of the calibrating straight, which is [0,l], the result can be written as follows:

$$\frac{\sigma_S - \sigma_1}{\sigma_S - \sigma_L} = e^{\frac{4fD_1}{\left(D_1^2 - d_1^2\right)} l} \tag{11}$$

where σ_L is the axial tensile stress in the tube section at the die opening; σ_1 is the tensile stress at the interface between the deformation zone and the calibrating

straight; l is the length of the calibrating straight.

From Eq. (11), the formula for the drawing stress σ_L is shown as follows:

$$\sigma_L = (\sigma_S - \sigma_1)e^{-\frac{4fD_1}{(D_1^2 - d_1^2)}l} + \sigma_s \tag{12}$$

The formula for the pulling force P is defined as:

$$P = \sigma_L \frac{\pi}{4}(D_1^2 - d_1^2) \tag{13}$$

Substituting Eq. (12) into Eq. (13), the pulling force P can be obtained:

$$P = ((\sigma_S - \sigma_1)e^{-\frac{4fD_1}{(D_1^2 - d_1^2)}l} + \sigma_s)\frac{\pi}{4}(D_1^2 - d_1^2) \tag{14}$$

3. Hollow sinking finite element analysis modeling

3.1 Principle of hollow sinking

The principle of hollow sinking is shown in Fig. 4. The mold consists of a drawing die and a clamp. During the forming process, the tube is fed forward at a constant speed with the collet at a certain value. The tube is extruded by the die to achieve a reduction in the diameter of the tube.

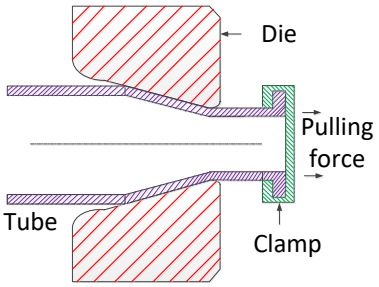

Fig.4 Hollow sinking schematic

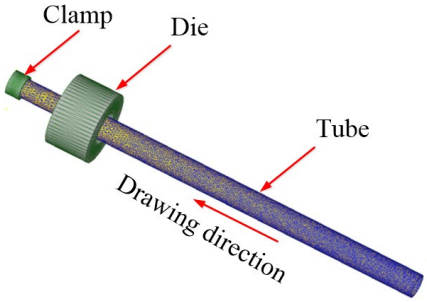

Fig.5 Hollow sinking finite element model

3.2 Establishment of the finite element model

Using Deform-3D finite element software, a null-drawing finite element model is established, as shown in Fig. 5. In this case, the tube size is ϕ2.0mm × 0.1mm × 140mm. Firstly, the mode selected for the analysis was heat transfer. Secondly, AISI-304 was selected as the material used for the tube, defined as a plastic body and divided absolutely with a tetrahedral mesh. The minimum size of the workpiece, i.e. a wall thickness of 0.1 mm, is used as the maximum cell size for meshing. In addition, the collet was defined as the main mold with the direction of motion in the -Y axis.

4. The influence of process parameters

4.1 Effect of drawing speed on the stress and fracture tendency of the tube

Supposing a friction coefficient of 0.08, an outer die angle of 6° and pulling speeds of 5mm/s, 15mm/s, 30mm/s, 60mm/s, 120mm/s and 240mm/s, respectively. Under these conditions, the relationship between the maximum Effective stress, damage factor, drawing force, and drawing speed are shown in Figs. 6 and 7.

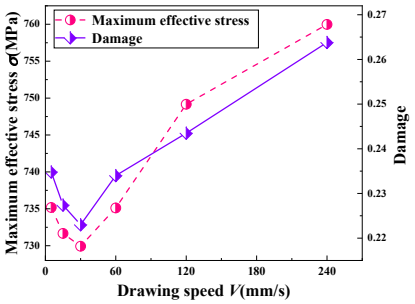

Fig.6 Variation of maximum effective stress and damage at different drawing speeds

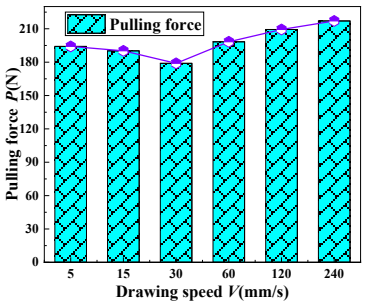

Fig.7 Graph of pulling force versus drawing speed

It can be seen from Fig. 6 and Fig. 7 that the maximum effective stress, damage and pulling force all decrease first and then increase with the increase of drawing speed. And when the drawing speed is 30mm/s, the minimum values of the maximum effective stress, damage, and pulling force were 729.93 MPa, 0.223, and 178.95 N, respectively. It can be seen that the maximum effective stress, damage and pulling force are larger at lower and higher drawing speeds and the tendency to fracture is also greater. This is because as the drawing speed increases, the deformation resistance of thin-walled tubes gradually increases, and the process hardening produced gradually increases, thus increasing the pulling force. When the drawing speed is higher, the strain rate is greater and the heat generated during drawing cannot be dissipated in time, thus the process hardening phenomenon is weakened and the pulling force is reduced. Therefore, the optimum drawing speed is 30 mm/s.

4.2 Effect of friction coefficient on strain and fracture tendency of tubes

Assuming an outer die angle of 6°, a pulling speed of 30 mm/s, and friction factors of 0.05, 0.08, 0.09, 0.1, and 0.14 respectively. Under these conditions, the relationship between the maximum equivalent stress, damage factor, pulling force, and friction coefficient are shown in Fig. 8 and Fig. 9.

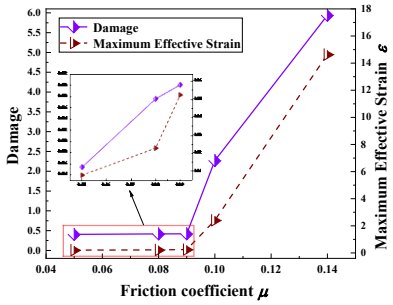

Fig.8 Plot of maximum effective stress and damage factor versus friction coefficient

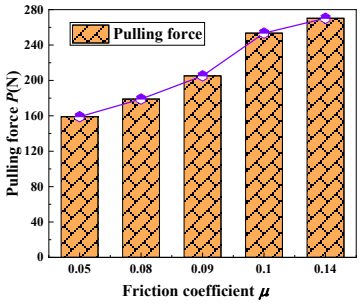

Fig.9 Graph of pulling force versus friction coefficient

It can be seen from Fig. 8 and Fig. 9 that the maximum effective strain, damage and pulling force all increase with the increase of friction coefficient. When the friction coefficient is 0.05, the values of the maximum effective stress, damage, and pulling force are the smallest, which are 0.4054, 0.208, and 159.02N respectively. At the friction coefficient of 0.1, the damage is 2.408. And the tube is damaged during the pulling process. The greater the coefficient of friction, the greater the friction. The greater the corresponding pulling force, the poorer the surface quality of the tube. Therefore, the optimum friction factor is 0.05.

4.3 Effect of outer die angle on the stress and fracture tendency of the tube

Suppose the friction coefficient is 0.08, the drawing speed is 30 mm/s and the outer die angle is 6°, 10°, 14°, and 18°, respectively. The maximum effective stress, damage factor, and drawing force about the outer die angle are shown in Fig. 10 and Fig. 11.

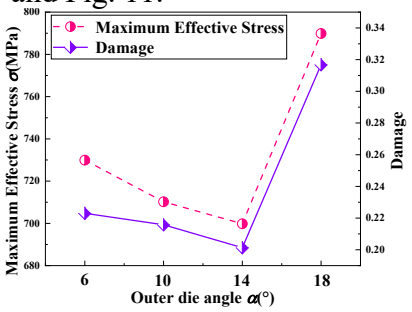

Fig.10 Plot of maximum effective stress and damage factor versus outer die angle

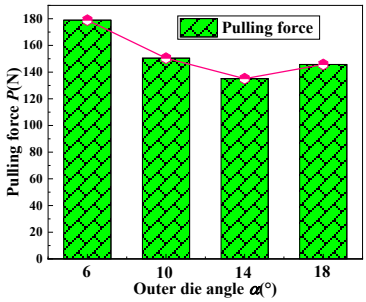

Fig. 11 Plot of pulling force versus outer die angle

It can be seen from Fig. 10 and Fig. 11 that the maximum effective stress, damage and pulling force all increase with the increase of the outer die angle. When the die angle is 14°, the maximum effective stress, damage and pulling force are the smallest, with minimum values of 699.82 MPa, 0.201, and 135.08N respectively. When the die angle is too small, the contact area between the tube and the die is too large, which in turn leads to an increase in the drawing force. When the die angle is too large, the flow line of the metal in the deformation area

turns sharply, which increases the unevenness of the metal deformation and increases the deformation work, thus causing an increase in the drawing force. The minimization of the drawing force was used as a criterion for the optimum process. Therefore, the optimum outer die angle is 14°.

5. Orthogonal optimization

The process parameters were selected as V=30mm/s, f=0.05, α=14°. The maximum effective stress diagram for thin-walled stainless steel tubes was obtained through simulation as shown in Fig. 12. It can be seen that: when the tube is pulled, the maximum effective stress increases in the compression zone, and then reaches a maximum in the sizing tape. Therefore, the sizing tape is subjected to the highest effective stress. The tube is most likely to be damaged in the sizing tape.

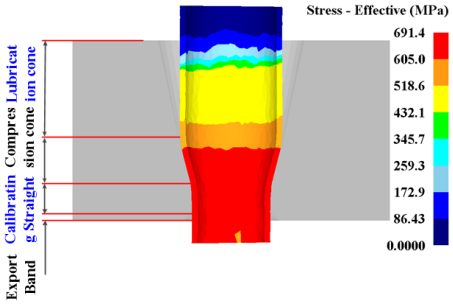

Fig.12 Effective stress cloud

Table.1

Results of the orthogonal test

Factors	Pulling speed V (mm/s)	Friction coefficient f	Outer die angle α(°)	Maximum effective stress σ(MPa)	Damage	Pulling force P(N)
1	20	0.03	12	656.50	0.14	119.49
2	20	0.05	14	669.00	0.18	136.47
3	20	0.07	16	751.70	0.49	216.57
4	30	0.03	14	681.60	0.17	125.32
5	30	0.05	16	738.80	0.4	189.36
6	30	0.07	12	679.50	0.16	121.35
7	40	0.03	16	732.10	0.46	203.42
8	40	0.05	12	670.00	0.13	115.65
9	40	0.07	14	689.00	0.19	139.86

5.1 Virtual orthogonal experimental design

Based on the above simulations using the DEFORMÂ® Software, it was found that by changing the values of the process parameters, only the effect of the process parameters alone on the maximum effective stress, damage, and pulling force of the tube hollow sinking could be demonstrated. Therefore, to obtain the primary and secondary order of the process parameters on the maximum effective

stress, damage, and pulling force of the tube hollow sinking, this paper uses the orthogonal optimization method to investigate these process parameters

5.2 Analysis results

The dimensional combinations and simulation results of the corresponding process parameters represented by the orthogonal sequential design combinations of drawing speed, friction coefficient, and outer die angle obtained using the SPSS are shown in Table 1.

5.3 Analysis of results

The methods of variance and extreme difference are the two main methods of analysis for orthogonal tests. The variance method distinguishes changes in the level of each factor of the test from fluctuations in the data caused by experimental error. The extreme difference method finds the optimum value of each factor, but does not take into account experimental error. Therefore, the results are analyzed using the variance method and the extreme difference method.

5.3.1Analysis of variance

In SPSS, the S-N-K method was applied for multiple comparisons. The results of the ANOVA are shown in Table 2.

Table.2

Analysis of Variance Data Table

	Source	Class III sum of squares	Freedom	Mean Square	F	Significance
Pulling speed	Maximum Effective stress	87.327	2	43.663	0.883	0.531
	Damage factors	0.001	2	0.001	1.140	0.467
	Pulling force	226.847	2	113.423	8.210	0.109
Friction coefficient	Maximum Effective stress	483.947	2	241.973	4.894	0.170
	Damage factors	0.003	2	0.001	2.953	0.253
	Pulling force	248.495	2	124.248	8.994	0.100
Outer die angle	Maximum Effective stress	9059.280	2	4529.640	91.613	0.011
	Damage factors	0.168	2	0.084	176.116	0.006
	Pulling force	12124.099	2	6062.050	438.820	0.002
Error	Maximum Effective stress	98.887	2	49.443		
	Damage factors	0.001	2	0.000		
	Pulling force	27.629	2	13.814		
Total	Maximum Effective stress	4375321.800	9			
	Damage factors	0.771	9			
	Pulling force	220408.059	9			

As can be seen from Table 2, for a given significance level α with a value of 0.05, the outer die angle has a significant effect on the simulation results, while the drawing speed and the friction coefficient have no significant effect on the simulation results. According to the F of the partial regression coefficient, the order of influence on the maximum effective stress, the damage and the pulling force are ranked as outer die angle > friction coefficient > drawing speed.

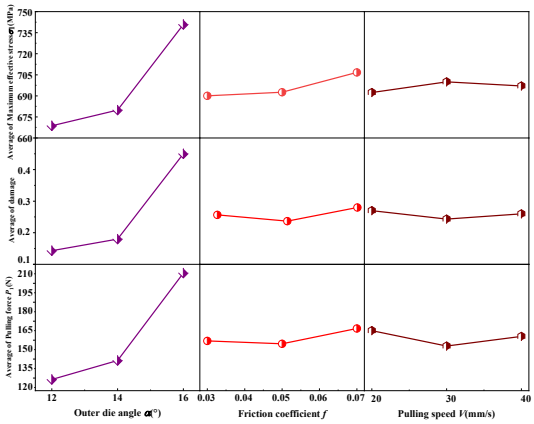

Fig. 13 Variation of the average of maximum effective stress, damage and pulling force for different process parameters

As can be seen from Fig. 13, the average of maximum effective stress, damage and pulling force are the smallest when the outer mold angle is 12°. The damage and pulling force are the smallest when the friction coefficient is 0.05. When the friction coefficient is 0.03, the average of the maximum effective stress is the smallest. When the drawing speed is 20mm/s, the average of the maximum effective stress is the smallest. The average of damage and the pulling force are the smallest when the pulling speed is 30 mm/s.

Therefore, taking the maximum effective stress as the variable, the optimum process parameters is the outer die angle of 12°, the friction coefficient of 0.03, and the drawing speed of 20mm/s. Taking the damage and pulling force as variables, the optimum process parameters are the outer die angle of 12°, the friction coefficient of 0.05, and the drawing speed of 30 mm/s.

5.3.2 Analysis of extreme differences

Table.3

Analysis of extreme differences Data Sheet

Test indicators	Maximum Effective stress σ/MPa			Damage			Pulling force P/N		
K_1	2077.2	2070.2	2006.0	0.81	0.77	0.43	472.53	448.23	356.49
K_2	2099.9	2077.8	2039.6	0.73	0.71	0.54	439.03	441.48	401.65
K_3	2091.1	2120.2	2222.6	0.78	0.84	1.35	458.93	477.78	609.35
k_1	692.4	690.1	668.7	0.27	0.26	0.14	157.51	149.41	118.83
k_2	700.0	692.6	679.9	0.24	0.24	0.18	146.34	147.16	133.88
k_3	697.0	706.7	740.9	0.26	0.28	0.45	152.98	159.26	203.12
R	7.6	16.6	72.2	0.03	0.04	0.31	11.17	12.1	69.23
Optimum level	V_1	f_1	α_1	V_2	f_2	α_1	V_2	f_2	α_1
Importance ranking		α, f, V			α, f, V			α, f, V	

The simulation results were analyzed according to the extreme difference analysis of the orthogonal experiment. The results of the experimental analysis are

shown in Table 3.

As can be seen from Table 3, the optimal level combinations and importance rankings from the variance method are identical to those obtained from the extreme difference, which justifies the conclusion. The optimal level combinations of the process parameters change according to the objectives of the optimization. Using the integrated balance method, the optimal combination of process parameters can be obtained that takes into account all objectives. The drawing speed of 30 mm/s, the friction factor of 0.05, and the outer die angle of 12° were selected as the optimal process combination.

5.4 Optimization analysis

Since the optimal process parameter combinations are not in the orthogonal table, the simulation is carried out with the optimal process parameter combinations. The results are shown in Table 4.

Table. 4

Comparison of maximum effective stress, damage and pulling force before and after optimization

	Maximum Effective stress σ/MPa	Damage	Pulling force P/N
Before optimization	691.4	0.2007	128.47
After optimization	664.7	0.1569	112.38
Ratio	3.8%	21.82%	12.52%

As can be seen from Table 4, comparing the process parameters before optimization, the maximum effective stress, damage and pulling force are reduced by 3.8%, 21.82% and 12.52% respectively. Therefore, the optimized process parameters are credible. And the results of the study can provide a theoretical basis for stainless steel tube hollow sinking.

6. Conclusion

(1) The maximum effective stress, damage and pulling force decrease and then increase as the drawing speed or outer die angle increases. Therefore, an appropriate drawing speed and outer die angle will improve the surface quality of the tube. The coefficient of friction is proportional to the maximum effective stress, damage and pulling force. Smaller friction coefficients will improve the surface quality of the tube.

(2) The variance and extreme difference analysis of the orthogonal analysis results show that: the outer die angle has a significant effect on the analysis results, while the drawing speed and friction coefficient have no significant effect on the analysis results. For the maximum effective stress, damage and pulling force of stainless steel tube hollow sinking, the outer die angle has the greatest influence, followed by the friction factor, and the drawing speed has the least influence

(3) The optimized combination of process parameters is the drawing speed of 30 mm/s, the friction coefficient of 0.05, and the outer die angle of 12°. With this

set of parameters, the maximum effective stress, damage and pulling force are reduced by 3.8%, 21.82% and 12.52% respectively.

Acknowledgement

This work was supported by a National Natural Resources grant for a controlled mechanism and experimental study of the proposed dynamics of high-speed ball spinning in precision tubes. (No. 51375325).

REFERENCES

[1] *S.Q. Liu, B.Y. Wang, W. Li, J.P. Liu*. "Investigation of cold drawing process of thin-walled ribbed steel tube". Journal of Manufacturing Processes, **vol.70**, 2021, pp.376-388.

[2] *R. Mojtaba, E. Majid, M. M. Javad*. "Development of bending of AISI 304L micro-tubes with micro-wire mandrel and investigation of its effective parameters". Journal of Manufacturing Processes, **vol.64**, 2021, pp.723–38.

[3] *C.C. Du*. "Application of Austenitic Stainless Steel in Industry". Process Equipment & Piping, no. 2, 2003, pp.54-57+4.

[4] *S.K. Lee, D.C. Ko, B.M. Kim, et al.* "A study on monobloc tube drawing for steering input shaft". Journal of Materials Processing Technology, **vol.191**, no. 1, 2007, pp.55-58.

[5] *K. Yoshida, H. Furuya.* "Mandrel drawing and plug drawing of shape-memory-alloy fine tubes used in catheters and stents". Journal of Materials Processing Technology, **vol. 153-154**, 2004, pp,145-150.

[6] *Q.Q. Luo*. Study on hot drawing process and microstructure and properties of magnesium alloy tubes, Master's thesis, Shenyang University of Technology,2014.

[7] *C. Wang, Z.Y. Yu, D. Ai, et al.* "Effects of Drawing Speed on the Hollow Sinking Process of the Zn Alloy Microtube". Materials Reports, **vol.32**, no.S2, 2018, pp.540-543.

[8] *L.L. Xie, P. Wang, Z.Y. Huang, et al.* "FE-simulation on Non-mandrel Drawing of Seamless Steel Tube". Hot Working Technology, **vol.40**, no.1, 2011, pp.99-101.

[9] *P. Jin, C.M. Liu, X.D. Yu, et al.* "Design of Drawing Process for HAI77-2 Brass Alloy Tubes with Hollow Sinking based on FEM Simulation". Nonferrous Metals Engineering & Research, **vol.37**, no.1, 2016, pp.23-26.

[10] *Y.F. Xia, Y. Tong, G,Z, Quan.* "Simulation Prediction on Wear of Non-mandrel Drawing Die of Alloy Tube". Hot Working Technology, **vol.39**, no.11, 2010, pp.9-11+15.

[11] *N.D. Farahani, A. Parvizi, A. Barooni, et al*. "Optimum curved die profile for tube drawing process with fixed conical plug". The International Journal of Advanced Manufacturing Technology, **vol.97**, no.1-4, 2018, pp.1–11.

[12] *S. Orhan, F. Oztürk, J. Gattmah*. "Effects of the semi die/plug angles on cold tube drawing with a fixed plug by FEM for AISI 1010 steel tube". Sakarya University Journal of Science, 2017, pp.1-1.

[13] *F. Boutenel, M. Delhomme, V. Velay, et al.* "Finite element modelling of cold drawing for high-precision tubes". Comptes Rendus Mécanique, **vol.346**, no.8, 2018, pp.665–677.

[14] *T. Pirling, A. Carrad`o, H. Palkowski*. "Residual stress distribution in seamless tubes determined experimentally and by FEM". Procedia Engineering, **vol.10**, no.C, 2011, pp,3080-3085.

[15] *G. Jabbar, O. Fahrettin, O. Sadettin*. "A new development of measurement technique for residual stresses generated by the cold tube drawing process with a fixed mandrel". The International Journal of Advanced Manufacturing Technology, **vol.108**, 2020, pp.3675-3687

[16] *J. Gattmah, F. Ozturk, S. Orhan*. "Experimental and finite element analysis of residual stresses in cold tube drawing process with a fixed mandrel for AISI 1010 steel tube". The International Journal of Advanced Manufacturing Technology, **vol.93**, no.1-4, 2017, pp.1229-1241.